Applied Catalysis B: Environmental 174–175 (2015) 471–476

Contents lists available at ScienceDirect

Applied Catalysis B: Environmental

journal homepage: www.elsevier.com/locate/apcatb

Fabrication and characterization of a *p*-type $Cu_3Nb_2O_8$ photocathode toward photoelectrochemical reduction of carbon dioxide

Sunao Kamimura, Naoya Murakami, Toshiki Tsubota, Teruhisa Ohno*

Department of Applied Chemistry, Faculty of Engineering, Kyushu Institute of Technology, 1-1 Sensuicho, Tobata, Kitakyushu 804-8550, Japan

ARTICLE INFO

Article history:
Received 19 March 2015
Accepted 22 March 2015
Available online 24 March 2015

Keywords:
Photocathode
Photocatalyst
Carbon dioxide
Photoelectrochemical reduction

ABSTRACT

We report a new *p*-type $Cu_3Nb_2O_8$ as a thin film photocathode, which was fabricated through spin-coating by a metal organic decomposition method. The *p*-type $Cu_3Nb_2O_8$ photocathode exhibited a strong cathodic photocurrent, and the incident photon-to-current conversion efficiency plot confirmed that the *p*-type $Cu_3Nb_2O_8$ photocathode has the ability to utilize the visible light ($\lambda <$ ca. 480 nm). Furthermore, we demonstrated photoelectrochemical reduction of carbon dioxide with the primary product being carbon monoxide by utilizing the *p*-type $Cu_3Nb_2O_8$ photocathode under AM 1.5 G solar light irradiation. From the results of Mott–Schottky analysis, UV–vis measurement and ultraviolet photoemission spectroscopy, the conduction band potential of *p*-type $Cu_3Nb_2O_8$ was estimated to be −1.21 V versus a normal hydrogen electrode (NHE) at pH 7 with its conduction band edge located at a more negative potential than the reduction potential of carbon dioxide to carbon monoxide. Although the cathodic photocurrent of the *p*-type $Cu_3Nb_2O_8$ photocathode gradually decayed with time, it recovered upon thermal annealing in air. This behavior suggests that the photocurrent response of the *p*-type $Cu_3Nb_2O_8$ photocathode is intimately related to variation of the valence state of copper ions. In this paper, the photoelectrochemical properties of the *p*-type $Cu_3Nb_2O_8$ photocathode are described in conjunction with optical, electrical and structural properties, and characteristics of the *p*-type $Cu_3Nb_2O_8$ photocathode for the photoelectrochemical reduction of carbon dioxide are discussed.

1. Introduction

The challenge of reducing carbon dioxide (CO_2) to chemical fuels has attracted considerable attention due to its potential for addressing the issues of depletion of fossil fuel and global warming [1–3]. Photoelectrochemical reduction utilizing a semiconductor photocathode is a promising approach for reducing CO_2 because it can proceed with a low electrical bias potential in contrast to electrochemical reduction due to a part or all of the energy being supplied by incident light. Photoelectrochemical reduction of CO_2 was first reported in 1978 by Halmann, who carried out a study in which CO_2 dissolved in an aqueous solution was converted to formic acid, formaldehyde and methanol by utilizing a *p*-type GaP photocathode under mercury lamp irradiation [4]. Inoue et al. investigated the use of several semiconductor powders in CO_2-saturated water under xenon lamp illumination, and they proposed that conversion processes of CO_2 to formic acid, formaldehyde and methanol were multi-electron reductions coupled with protons in an aqueous solution [5]. Based on these breakthroughs, most of the works on photoelectrochemical reduction of CO_2 have focused on proton-coupled multi-electron reduction utilizing *p*-type III–V and II–VI semiconductor photocathodes (e.g., InP and GaAs) [6,7]. Although *p*-type III–V and II–VI semiconductors exhibit remarkable photocurrent responses for reducing CO_2, they are unstable under light illumination and need excessively high overpotential for the reduction of CO_2 [8–10].

Recently, research in this field has resulted in the design and development of a new class of photocathodes utilizing metal-oxide, oxynitride and sulfide semiconductors [11–13]. Metal-oxide semiconductors have attracted much attention as promising candidates of a photocathode for photoelectrochemical reduction of CO_2 because of their superior corrosion resistance. Metal-oxide semiconductors are typically classified into two categories, *n*-type semiconductors and *p*-type semiconductors, depending on whether the majority carriers are electrons or holes, respectively. To utilize a photocathode for photoelectrochemical reduction of CO_2, a *p*-type semiconducting metal oxide is essential. A *p*-type semiconducting metal oxide acts as a photocathode because photo-excited electrons created in the conduction band (CB) by irradiation of incident light are more energetic than the band gap, while an

* Corresponding author. Tel.: +81 938843318.
E-mail address: tohno@che.kyutech.ac.jp (T. Ohno).

http://dx.doi.org/10.1016/j.apcatb.2015.03.034
0926-3373/

n-type semiconductor acts as a photoanode as holes are created in the valence band (VB) by irradiation of incident light [14]. To date, much effort has been devoted to exploring *p*-type semiconducting metal oxides functioning as photocathodes for photoelectrochemical reduction of CO_2; however, that reports have been limited to CuO, Cu_2O, Co_3O_4, $CaFe_2O_4$, and $CuFeO_2$ [15–18]. Therefore, we focused on the development of a new *p*-type metal-oxide semiconductor for photoelectrochemical reduction of CO_2.

After examining a number of *p*-type semiconducting metal oxides, we successfully developed a new *p*-type $Cu_3Nb_2O_8$ photocathode that was fabricated through spin coating by a metal organic decomposition method. The $Cu_3Nb_2O_8$ photocathode exhibited a strong cathodic photocurrent with irradiation of AM 1.5 G solar-simulated light, leading to photoelectrochemical reduction of CO_2 with the primary product being carbon monoxide (CO). As far as we know, there has been no report on photoelectrochemical characteristics of the *p*-type $Cu_3Nb_2O_8$ and its photoelectrochemical reduction of CO_2. In this paper, we present the photoelectrochemical properties of the *p*-type $Cu_3Nb_2O_8$ photocathode in conjunction with optical, electrical and structural properties, and we discuss its photoclectrochemical reduction of CO_2.

2. Experimental

2.1. Fabrication

Three different series of samples were fabricated. One series was fabricated onto a metal Ti substrate by the spin coating method for analysis of linear sweep voltammetry and chronoamperometry measurements. The metal Ti substrate (15 mm × 40 mm, thickness: 0.1 mm, Nilaco Co.) was ultrasonically cleaned in ethanol and acetone each for 1 h. Then 0.4 M CuO precursor solution (SYM-Cu04, Kojundo Chemical Lab, Co.) and 0.5 M $NbO_{2.5}$ precursor solution (SYM-Nb05, Kojundo Chemical Lab, Co.) as starting reagents were weighed precisely to molar ratios of Cu: Nb = 1.5:1.0 and mixed thoroughly. The mixture was then deposited on the metal Ti substrate and accelerated rapidly in air. The spin speed was 1000 revolutions per minute and spin time was 30 s. The prepared thin film of the mixture on the metal Ti substrate was calcined at 873 K for 2 h in air. It should be noted that I–V characteristics confirmed ohmic contact between $Cu_3Nb_2O_8$ and the calcined Ti substrate (Figure S1, Supporting information). The second series was fabricated on a quartz substrate by the spin coating method for analysis of UV–vis measurements. The quartz substrate (25 mm × 25 mm, thickness: 1 mm) was ultrasonically cleaned in acetone and ethanol each for 1 h. The precursor solutions mentioned above were deposited on the quartz substrate and then accelerated rapidly in air. The spin speed was 1000 revolutions per minute and spin time was 30 s. The prepared thin film of the mixture on the quartz substrate was calcined at 873 K for 2 h in air. The third series was fabricated on a quartz substrate on which platinum was deposited at ca. 500 nm by magnetron sputtering (SC-701HMCII, Sanyu Electron Co.) for Mott–Schottky analysis. The precursor solutions were deposited on the Pt/quartz substrate and then accelerated rapidly in air. The spin speed was 1000 revolutions per minute and spin time was 30 s. The prepared thin film of the mixture on the quartz substrate was calcined at 873 K for 2 h in air. Spin coating was carried out 10 times for Mott–Schottky analysis.

2.2. Characterization

The crystalline phase of $Cu_3Nb_2O_8$ was characterized by using a powder X-ray diffraction (XRD) instrument (MiniFlex II, Rigaku Co.) with CuKα (λ = 1.5418 Å) radiation (cathode voltage: 30 kV, current: 15 mA). The absorption spectrum was acquired at room temperature with a UV–vis spectrometer (UV-2600, Shimadzu Co.). Mott–Schottky analysis was carried out by using an electrochemical analyzer (604D, ALS Co.) with a $Cu_3Nb_2O_8$ electrode, platinum electrode, Ag/AgCl electrode and non-CO_2 bubbled 0.5 M $NaHCO_3$ solution (pH 8.6) used as a working electrode, counter electrode, reference electrode and electrolyte, respectively. X-ray photoelectron spectroscopy (XPS) measurements were also performed using a Kratos AXIS Nova spectrometer (Shimazu Co.) with a monochromatic Al Kα X-ray source. The binding energy was calibrated by taking the carbon (C) 1s peak of contaminant carbon as a reference at 248.7 eV.

2.3. Photoelectrochemical measurements

Linear sweep voltammetry and chronoamperometry measurements were carried out by using an automatic polarization system (HSV-100, Hokuto Denko Co.) with a three-electrode system, in which a $Cu_3Nb_2O_8$ electrode, a glassy carbon electrode and a silver–silver chloride (Ag/AgCl) electrode were used as a working electrode, counter electrode and reference electrode, respectively. The electrolyte used was 0.5 M $NaHCO_3$ solution, which was bubbled with CO_2 gas for 30 min to remove dissolved air. The pH of 0.5 M $NaHCO_3$ solution after bubbling with CO_2 gas for 30 min was pH 7.3. It should be noted that the CO_2 gas continuously flowed into the reactor during the linear sweep. The light source used was a solar-simulated system (PEC-L15, Peccell Tech., Inc.). The light intensity of the solar-simulated light was determined by utilizing a thermopile power meter (ORION-TH), and the intensity was 100 mW/cm^2. Incident photon to current efficiency (IPCE) measurement was carried out by using an automatic polarization system (HSV-100, Hokuto Denko Co.) and light-emitting diodes as the light source peaking at 365 nm, 415 nm, 455 nm, 470 nm, 505 nm, 530 nm and 720 nm (light intensity: 1.0 mW/cm^2). The IPCE at each irradiation wavelength was calculated by the following equation:

$$\mathrm{IPCE}\,(\%) = \frac{1239.7 \times J\left(\frac{\mathrm{mA}}{\mathrm{cm}^2}\right)}{\lambda\,(\mathrm{nm}) \times I\left(\frac{\mathrm{mW}}{\mathrm{cm}^2}\right)} \times 100,$$

where J is photocurrent density of the $Cu_3Nb_2O_8$ electrode, λ is irradiation wavelength of the light-emitting diodes, and I is irradiation intensity of the light-emitting diodes.

2.4. Evaluation of reduction products

Photoelectrochemical reduction of CO_2 to CO over the $Cu_3Nb_2O_8$ electrode was carried out by using an automatic polarization system (HSV-100, Hokuto Denko Co.) with a three-electrode photoelectrochemical cell system in which the $Cu_3Nb_2O_8$ electrode, glassy carbon electrode and silver–silver chloride (Ag/AgCl) electrode were used as a working electrode, counter electrode and reference electrode, respectively. After CO_2 bubbling for 30 min, the cell was sealed and irradiated by AM 1.5 G solar-simulated light for 20 min. The gaseous CO_2 reduction products, including CO and CH_4, were detected by gas chromatography (490 Micro GC, Agilent Technology Co.). The liquid CO_2 reduction product, formic acid (HCOOH), was detected by using single-channel ion chromatography (ICS900, Thermo Fisher Scientific Inc.), and other products including methanol (CH_3OH), ethanol (C_2H_5OH), and formaldehyde (HCOH) were detected by gas chromatography (G-3500, Hitachi Co.) with a DB-WAXetr column (122-7332, Agilent Co.).

3. Results and discussion

Fig. 1(a) shows the XRD pattern of $Cu_3Nb_2O_8$. The XRD pattern corresponded to the powder diffraction file for the triclinic

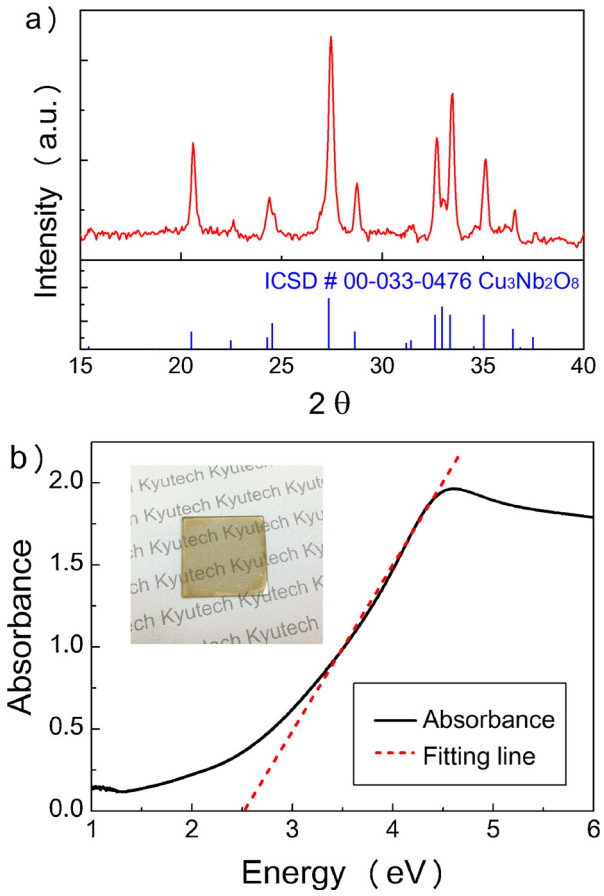

Fig. 1. (a) XRD pattern of the *p*-type $Cu_3Nb_2O_8$ photocathode together with standard PDF data for $Cu_3Nb_2O_8$ (00-033-0476). (b) UV–vis spectrum of *p*-type $Cu_3Nb_2O_8$ on the quartz glass.

phase of $Cu_3Nb_2O_8$ (JCPDS 00-033-0476), indicating that $Cu_3Nb_2O_8$ polycrystalline can be synthesized. The thickness of the $Cu_3Nb_2O_8$ polycrystalline layer was estimated from a cross-section SEM image to be approximately 145 nm (Figure S2, Supporting information). Fig. 1(b) shows the UV–vis spectrum of the $Cu_3Nb_2O_8$ in the photon energy range between 1 eV and 6 eV. As shown in the inset picture, the obtained $Cu_3Nb_2O_8$ on the quartz glass was a dark yellow color. The band gap was found by extrapolation of the absorption band edge, and it was estimated to be 2.5 eV.

To clarify the flat band potential (E_{fb}) of $Cu_3Nb_2O_8$, Mott–Schottky analysis was carried out by using an alternating current (AC) electrochemical impedance method at 0.5 kHz, 1 kHz and 2 kHz with AC 5 mV of amplitude in a non-CO_2 bubbled 0.5 M $NaHCO_3$ solution (pH 8.6), and the resulting Mott–Schottky plots are shown in Fig. 2(a). Negative slopes were observed at all AC frequencies, suggesting that $Cu_3Nb_2O_8$ behaves as a *p*-type semiconductor. In the case of *p*-type semiconductors, E_{fb} is generally located near the VB, and it can be estimated from the intersection of a plot of $1/C^2$ against E by the following equation [19]:

$$\frac{1}{C^2} = \frac{2}{e\epsilon\epsilon_0 N}\left(E - E_{fb} - \frac{kT}{e}\right),$$

where C is capacitance, e is the electron charge, ϵ is the dielectric constant, ϵ_0 is permittivity of vacuum, N is an acceptor density, E is the electrode potential, E_{fb} is the flat band potential, k is the Boltzmann constant, and T is temperature. As shown in Fig. 2(a), the *x*-axis intersection was $E = +1.05$ V versus Ag/AgCl (pH 8.6) for all frequencies (0.5 kHz, 1 kHz, and 2 kHz) and can be used to determine E_{fb} from the above equation $E = E_{fb} - kT/e$. This calculation showed that E_{fb} was approximately +1.11 V versus Ag/AgCl (pH 7) by correcting the solution pH using the relation $E = E_0 - 0.059$ V(pH). This result indicated that the VB potential and CB potential of *p*-type $Cu_3Nb_2O_8$ are approximately +1.31 V and −1.21 V versus a normal hydrogen electrode (NHE) at pH 7, respectively. Fig. 2(b) shows the band potential diagram for *p*-type $Cu_3Nb_2O_8$, together with the thermodynamic potentials for CO_2 reduction to various reduction products versus NHE at pH 7. As shown in this figure, the CB potential of the *p*-type $Cu_3Nb_2O_8$ was higher than the redox potential of CO_2, suggesting that photoelectrochemical reduction of CO_2 is possible by utilizing the *p*-type $Cu_3Nb_2O_8$ photocathode.

Fig. 3(a) shows linear sweep voltammetry of the *p*-type $Cu_3Nb_2O_8$ photocathode in 0.5 M $NaHCO_3$ solution bubbled with CO_2 gas with irradiation of AM 1.5 G solar-simulated light. The *p*-type $Cu_3Nb_2O_8$ photocathode exhibited a cathodic photocurrent in response to irradiation of solar light, and the cathodic photocurrent density reached −0.18 mA/cm^2 at −0.30 V applied potential versus Ag/AgCl. As shown in the inset figure, the onset potential of the *p*-type $Cu_3Nb_2O_8$ photocathode was estimated to be approximately +0.25 V versus Ag/AgCl (pH 7.3). The onset potential is generally close to E_{fb}; however, the *p*-type $Cu_3Nb_2O_8$ photocathode showed that the potential difference between onset potential and E_{fb} was ca. −1 V. This large discrepancy between onset potential and E_{fb} is thought to be caused mainly by slow kinetics for proton-coupled multi-electron reduction of CO_2 that results in electron accumulation on the surface of the *p*-type $Cu_3Nb_2O_8$ photocathode, and then subsequent surface recombination occurs until sufficient applied potential is achieved for an appreciable charge transfer across the *p*-type $Cu_3Nb_2O_8$/$NaHCO_3$ electrolyte junction, similar to α-Fe_2O_3 and *p*-type GaP [20–23]. Thus, in the case of

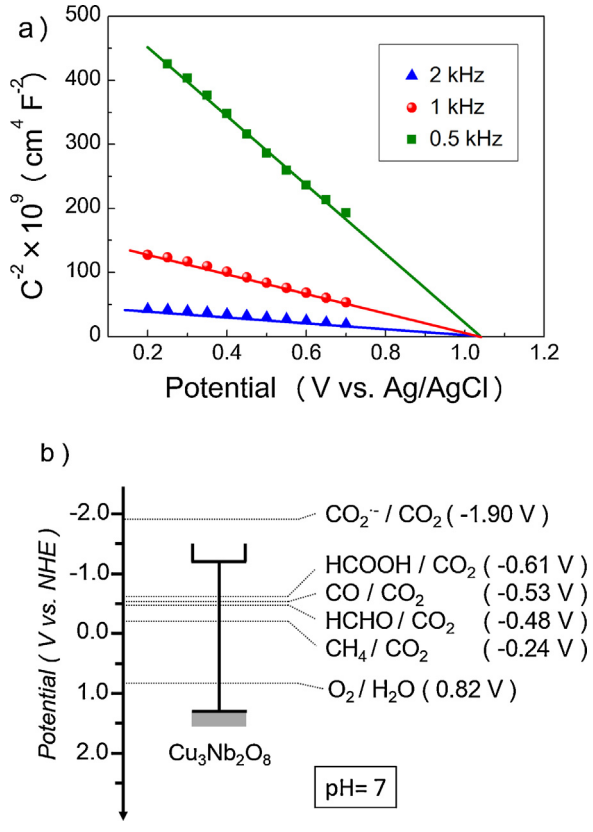

Fig. 2. (a) Mott–Schottky plots at 0.5 kHz, 1 kHz and 2 kHz measured under dark conditions. (b) Position of the conduction band and valence band of *p*-type $Cu_3Nb_2O_8$ photocathode together with the redox potential of various reduction products/CO_2.

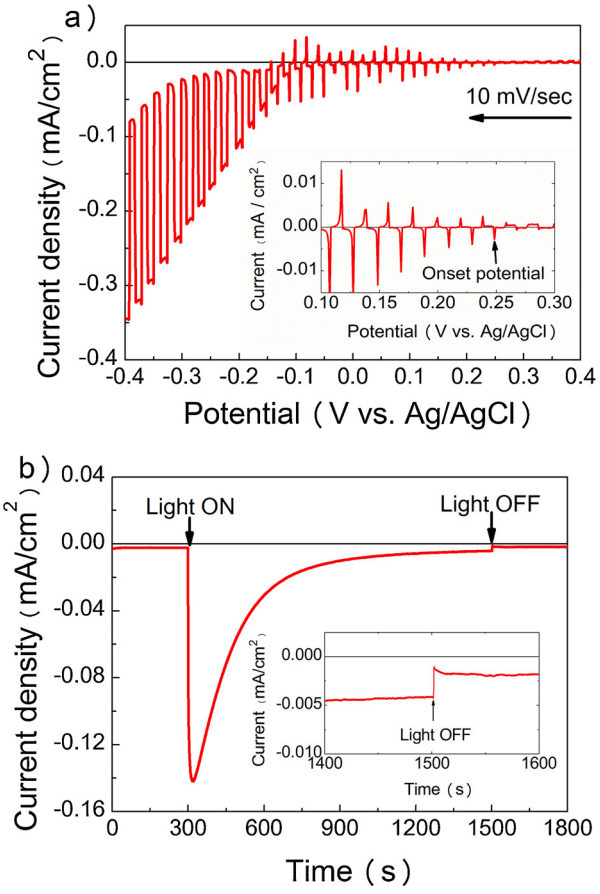

Fig. 3. (a) Linear sweep voltammetry of *p*-type $Cu_3Nb_2O_8$ photocathode under "chopped" AM 1.5 G solar-simulated light irradiation. The inset shows a reproduction of a part of the same figure at a finer resolution. The electrolyte is CO_2-bubbled aqueous $NaHCO_3$ solution (pH 7.3) (b) Chronoamperometry of *p*-type $Cu_3Nb_2O_8$ photocathode with applied potential at −0.2 V versus Ag/AgCl under AM 1.5 G solar-simulated light illumination.

the $Cu_3Nb_2O_8$ photocathode, efficient electron–hole separation and charge transfer should only require applied potential from +0.25 V versus Ag/AgCl toward negative potential. Fig. 3(b) shows the time dependence of a cathodic photocurrent of the *p*-type $Cu_3Nb_2O_8$ photocathode in 0.5 M $NaHCO_3$ solution bubbled with CO_2 gas at −0.20 V applied potential versus Ag/AgCl. When AM 1.5 G solar-simulated light was irradiated to the *p*-type $Cu_3Nb_2O_8$ photocathode, the cathodic photocurrent rapidly increased and then gradually decreased with time. After 20 min, the photocurrent was decreased to approximately 98% of that in the initial state. However, the XRD pattern of the *p*-type $Cu_3Nb_2O_8$ photocathode barely changed after the chronoamperometry measurement (Figure S3, Supporting information). This result implies that photocorrosion or reduction of the *p*-type $Cu_3Nb_2O_8$ photocathode itself might occur, as will be discussed later in detail. To clarify the irradiation wavelength dependence of a cathodic photocurrent in the *p*-type $Cu_3Nb_2O_8$ photocathode, the action spectrum was acquired by determining the IPCE at −0.3 V versus Ag/AgCl. Fig. 4 shows the IPCE action spectrum of the *p*-type $Cu_3Nb_2O_8$ photocathode in 0.5 M $NaHCO_3$ solution bubbled with CO_2 gas, together with its absorption spectrum. The IPCE action spectrum was consistent with the absorption spectrum, and each IPCE was approximately 1.4%, 4.3%, and 6.7% with an irradiation wavelength at 505 nm, 415 nm, and 365 nm, respectively. These results indicate that the *p*-type $Cu_3Nb_2O_8$ photocathode responds to visible-light irradiation (also sunlight illumination), leading to electron–hole generation

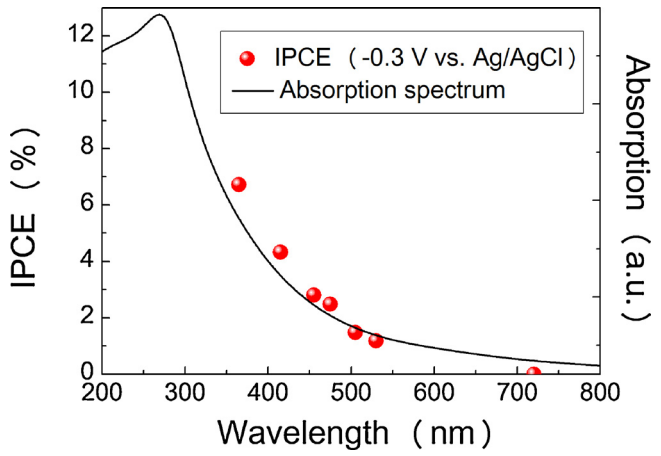

Fig. 4. IPCE plots of *p*-type $Cu_3Nb_2O_8$ photocathode with applied potential at −0.3 V versus Ag/AgCl in CO_2-bubbled $NaHCO_3$ solution, together with absorption spectrum of the *p*-type $Cu_3Nb_2O_8$.

and charge transfer in the $Cu_3Nb_2O_8$/$NaHCO_3$ electrolyte junction to drive CO_2 reduction.

Photoelectrochemical reduction of CO_2 to CO over the *p*-type $Cu_3Nb_2O_8$ photocathode was measured at different applied potentials ranging between 0 V and −0.4 V versus Ag/AgCl, and the results are shown in Fig. 5. It should be noted that AM 1.5 G solar-simulated light was irradiated for 20 min, based on the results of the chronoamperometry measurement (refer to Fig. 3(b)). As shown in this figure, CO evolution increased with an increase in the applied potential, the tendency of which corresponded to the results of the photocurrent response of the *p*-type $Cu_3Nb_2O_8$ photocathode with applied potential (refer to Fig. 3(a)), suggesting that a cathodic photocurrent arose from the photoelectrochemical reduction of CO_2 to CO. The thermodynamic potential for photoelectrochemical reduction of CO_2 to CO in the presence of protons is generally explained by the following equation:

$$CO_2 + 2H^+ + 2e^- \rightarrow CO + H_2O (-0.53\,V versus NHE at pH 7).$$

Here, the conduction potential of the *p*-type $Cu_3Nb_2O_8$ photocathode was estimated to be −1.21 V versus NHE at pH 7, and photoelectrochemical reduction of CO_2 to CO over the *p*-type $Cu_3Nb_2O_8$ photocathode was therefore reasonable. However, the calculated faradic efficiency for CO evolution was approximately 9% at −0.20 V applied potential versus Ag/AgCl, indicating that

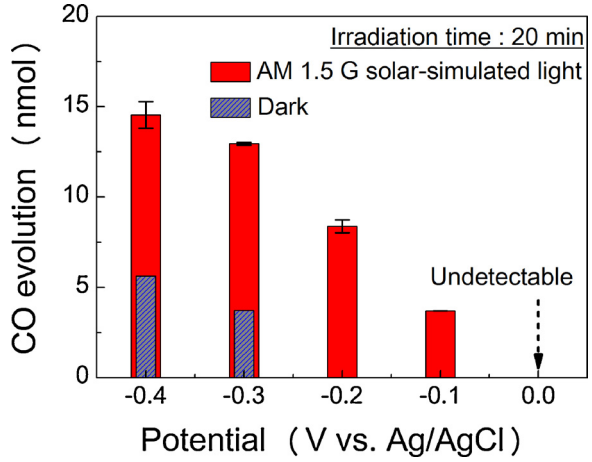

Fig. 5. Photoelectrochemical reduction of CO_2 to CO over *p*-type $Cu_3Nb_2O_8$ photocathode at different applied potential ranging between 0 V and −0.4 V versus Ag/AgCl.

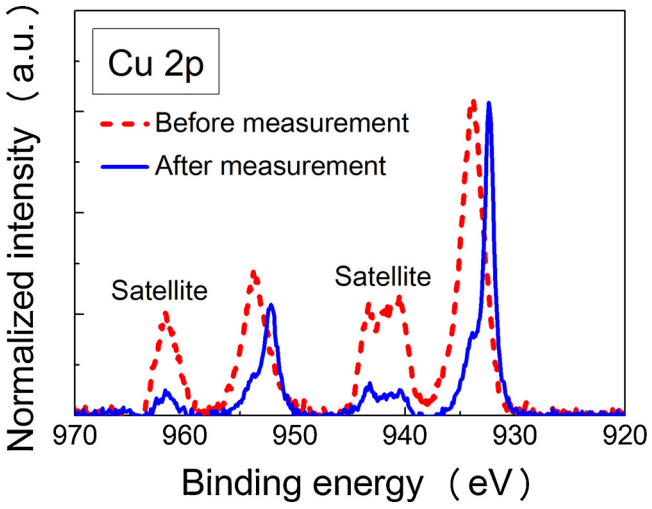

Fig. 6. XPS spectra of Cu 2p of the *p*-type $Cu_3Nb_2O_8$ photocathode obtained before and after chronoamperometry measurement at −0.2 V versus Ag/AgCl in CO_2-bubbled $NaHCO_3$ solution.

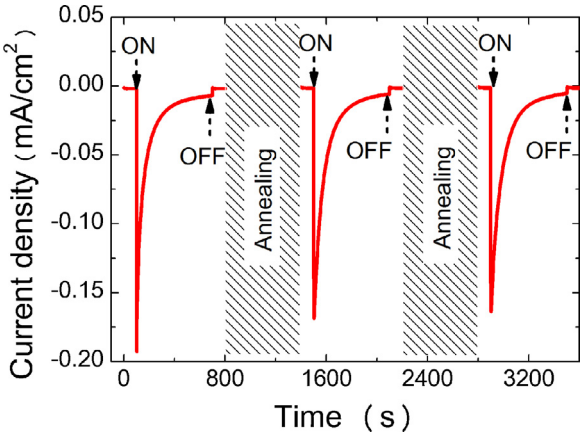

Fig. 7. Chronoamperometry of *p*-type $Cu_3Nb_2O_8$ photocathode in 0.5 M $NaHCO_3$ bubbled with CO_2 gas at −0.20 V applied potential versus Ag/AgCl measured up to 3 cycles. The annealing was carried out by using a hot plate with temperature kept at 823 K in air.

most of the cathodic photocurrent of the *p*-type $Cu_3Nb_2O_8$ photocathode was consumed to produce other chemical products or for reduction of the electrode itself. Taking into consideration the fact that other chemical products, including formic acid, methane, formaldehyde, methanol and ethanol, were not observed from the results of gas chromatography and ion chromatography analysis, it is highly possible that a cathodic photocurrent leads to photocorrosion or reduction of the *p*-type $Cu_3Nb_2O_8$ photocathode itself. Previously, Paracchino et al. and Huang et al. revealed that photocorrosion of copper oxides (Cu_2O) was ascribed to variation of the valence state of copper from Cu (I) to Cu (0) and Cu (II) species [24,25]. To investigate the valence state of copper in the *p*-type $Cu_3Nb_2O_8$ photocathode, XPS measurement was done before and after chronoamperometry measurement, and the results of the Cu 2p spectra are shown in Fig. 6. Before chronoamperometry measurement, major peaks at 933.8 eV and 953.8 eV were observed, and these peaks were attributed to typical values of Cu $2p_{3/2}$ and $2p_{1/2}$, respectively. Divalent copper Cu (II) compounds generally exhibit strong satellite peaks with higher binding energy sides compared with each of the copper $2p_{3/2}$ and $2p_{1/2}$ lines [26,27]. As clearly shown in this figure, strong satellite peaks were observed as an indication of the presence of Cu (II) species in the *p*-type $Cu_3Nb_2O_8$ photocathode before chronoamperometry measurement. On the other hand, the peak profile of the Cu 2p XPS spectrum was clearly changed after chronoamperometry measurement; strong sharp peaks located at 932.4 eV and 952.2 eV were newly observed. These peaks were identified to be monovalent copper Cu (I) and/or metal copper Cu (0) [28], indicating that Cu (II) species in the *p*-type $Cu_3Nb_2O_8$ photocathode was reduced to Cu (I) and/or Cu (0) species by chronoamperometry measurements, resulting in a decay of the cathodic photocurrent with time, as shown in Fig. 3(b). However, taking into consideration that the Nb 3d and O 1s XPS spectrum was not changed by chronoamperometry measurements (Figure S4, Supporting information), it is highly possible that Nb and O ions in the *p*-type $Cu_3Nb_2O_8$ were stable. It should be emphasized that the decay of the cathodic photocurrent recovered when the *p*-type $Cu_3Nb_2O_8$ photocathode was thermally annealed in air. Fig. 7 shows the results of chronoamperometry of the *p*-type $Cu_3Nb_2O_8$ photocathode in 0.5 M $NaHCO_3$ solution bubbled with CO_2 gas at −0.20 V applied potential versus Ag/AgCl measured up to 3 cycles. The incident light source was AM 1.5 G solar-simulated light (intensity: 100 mW/cm^2). In the first cycle, a cathodic photocurrent rapidly increased when incident light was irradiated, followed by a decrease with time due to the reduction of Cu (II) in the *p*-type $Cu_3Nb_2O_8$ photocathode, which is similar response behavior to that shown in Fig. 3(b). After this measurement, the *p*-type $Cu_3Nb_2O_8$ photocathode was annealed for 10 min by using a hot plate, on which the heating temperature was kept at 873 K. In the second cycle, a similar chronoamperometry response was observed. The same test was repeated three times in succession. The decay of the cathodic photocurrent with time followed by its recovery with thermal annealing, as clearly shown in this figure, indicated that the valence state of copper in the *p*-type $Cu_3Nb_2O_8$ photocathode recovered back from Cu (0) and Cu (I) to Cu (II) species (Figure S5, Supporting information). Thus, the *p*-type $Cu_3Nb_2O_8$ photocathode exhibited a cathodic photocurrent with irradiation of visible light and AM 1.5 G solar-simulated light with a part of the cathodic photocurrent arising from the photoelectrochemical reduction of CO_2 to CO and the other part leading to reduction of the *p*-type $Cu_3Nb_2O_8$ photocathode itself. The reduction of the *p*-type $Cu_3Nb_2O_8$ photocathode was ascribed to the variation of valence state of copper from Cu (II) to Cu (0) and Cu (I) species, while it was recovered by thermal annealing in air. Although there is no clear evidence, we speculated that the reduction of the electrode of the *p*-type $Cu_3Nb_2O_8$ photocathode can be prevented by a protecting layer, electron collecting layer, and deposition of metallic particles, similar to a Cu_2O/ZnO:Al/Pt photocathode [29,30].

4. Conclusions

We successfully developed a new series of p-type $Cu_3Nb_2O_8$ photocathode that could be fabricated through spin coating by a metal organic decomposition method. The *p*-type $Cu_3Nb_2O_8$ photocathode exhibited a relatively strong cathodic photocurrent with irradiation of AM 1.5 G solar-simulated light, and the cathodic photocurrent density reached −0.18 mA/cm^2 at −0.30 V applied potential versus Ag/AgCl. Furthermore, we demonstrated photoelectrochemical reduction of CO_2 by utilizing the *p*-type $Cu_3Nb_2O_8$ photocathode in an aqueous CO_2-bubbled $NaHCO_3$ solution (pH 7.3). The only reduction product observed was carbon monoxide with a calculated faradic efficiency of 9% at −0.20 V applied potential versus Ag/AgCl, and other chemical products including formic acid, methane, formaldehyde, methanol and ethanol were not observed. The XPS analysis confirmed reduction of the *p*-type $Cu_3Nb_2O_8$ photocathode itself by the photoelectrochemical measurement, which was ascribed to variation of the valence state of copper from Cu(II) to Cu(0), Cu(I). Although we found that the

reduction of the *p*-type $Cu_3Nb_2O_8$ photocathode could be recovered by thermal annealing in air, other aspects such as the protecting layer, electron collecting layer, and deposition of metallic particles are not clear yet. Further research is required to improve the CO_2 conversion efficiency of the *p*-type $Cu_3Nb_2O_8$ photocathode and understand the CO_2 reduction mechanism in depth.

Acknowledgements

The authors thank to Prof. Tetsuya Haruyama, Prof. Yoichi Shimizu of Kyushu Institute of Technology, and Takeshi Fukuma of Kanazawa Univ. for their valuable contributions to this study. This work has been supported by a grant from Advanced Catalytic Transformation program for Carbon utilization (ACT-C), and Japan Science and Technology Agency (JST).

Appendix A. Supplementary data

Supplementary data associated with this article can be found, in the online version, at http://dx.doi.org/10.1016/j.apcatb.2015.03.034.

References

[1] S.C. Roy, O.K. Varghese, M. Paulose, C.A. Grimes, ACS Nano 4 (2010) 1259.
[2] M. Tahir, N.S. Amin, Energy Convers. Manage. 76 (2013) 194.
[3] S.N. Habisreutinger, L. Schmidt-Mende, J.K. Stolarczyk, Angew. Chem. Int. Ed. 52 (2013) 7372.
[4] M. Halmann, Nature 275 (1978) 115.
[5] T. Inoue, A. Fujishima, S. Konishi, K. Honda, Nature 277 (1979) 637.
[6] S. Sato, T. Arai, T. Morikawa, K. Uemura, T.M. Suzuki, H. Tanaka, T. Kajino, J. Am. Chem. Soc. 133 (2011) 15240.
[7] S. Kaneco, H. Katsumata, T. Suzuki, K. Ohta, Chem. Eng. J. 116 (2006) 227.
[8] B.A. Blajeni, M. Halmann, J. Manassen, Sol. Energy Mater. 8 (1983) 425.
[9] J. Schefold, J. Phys. Chem. 96 (1992) 8692.
[10] E.E. Barton, D.M. Rampulla, A.B. Bocarsly, J. Am. Chem. Soc. 130 (2008) 6342.
[11] M. Schreier, P. Gao, M.T. Mayer, J. Luo, T. Moehl, M.K. Nazeeruddin, S.D. Tilley, M. Grätzel, Energy Environ. Sci. 8 (2015) 855.
[12] K. Sekizawa, K. Maeda, K. Domen, K. Koike, O. Ishitani, J. Am. Chem. Soc. 135 (2013) 4596.
[13] T. Arai, S. Tajima, S. Sato, K. Uemura, T. Morikawa, T. Kajino, Chem. Commun. 47 (2011) 12664.
[14] N.K. Awad, E.A. Ashour, N.K. Allam, J. Renew. Sustain. Energy 6 (2014) 022702-1.
[15] G. Ghadimkhani, N.R. de Tacconi, W. Chanmanee, C. Janaky, K. Rajeshwar, Chem. Commun. 49 (2013) 1297.
[16] X. Huang, T. Cao, M. Liu, G. Zhao, J. Phys. Chem. C 117 (2013) 26432.
[17] J. Gu, A. Wuttig, J.W. Krizan, Y. Hu, Z.M. Detweiler, R.J. Cava, A.B. Bocarsly, J. Phys. Chem. C 117 (2013) 12415.
[18] Y. Matsumoto, M. Obata, J. Hombo, J. Phys. Chem. 98 (1994) 2950.
[19] L. Kavan, M. Grätzel, S.E. Gilbert, C. Klemenz, H.J. Scheel, J. Am. Chem. Soc. 118 (1996) 6716.
[20] G. Horowitz, Appl. Phys. Lett. 40 (1982) 409.
[21] H. Flaisher, R. Tenne, M. Halmann, J. Electroanal. Chem. 402 (1996) 97.
[22] S.D. Tilly, M. Cornuz, K. Sivula, M. Grätzel, Angew. Chem. 122 (2010) 6549.
[23] J. Gu, Y. Yan, J.W. Krizan, Q.D. Gibson, Z.M. Detweiler, R.J. Cava, A.B. Bocarsly, J. Am. Chem. Soc. 136 (2014) 830.
[24] A. Paracchino, V. Laporte, K. Sivula, M. Grätzel, E. Thimsen, Nat. Mater. 10 (2011) 456–461.
[25] L. Huang, F. Peng, H. Yu, H. Wang, Solid State Sci. 11 (2009) 129.
[26] S. Poulston, P.M. Parlett, P. Stone, M. Bowker, Surf. Interface Anal. 24 (1996) 811.
[27] Y. Nakabayashi, M. Nishikawa, Y. Nosaka, Electrochem. Acta 125 (2014) 191.
[28] S.W. Lee, Y.S. Lee, J. Heo, S.C. Siah, D. Chua, R.E. Brandt, S.B. Kim, J.P. Mailoa, T. Buonassisi, R.G. Gordon, Adv. Energy Mater. 4 (2014) 1301916.
[29] S.D. Tilly, M. Schreier, J. Azevedo, M. Stefik, M. Grätzel, Adv. Funct. Mater. 24 (2014) 303.
[30] Y. Kou, S. Nakatani, G. Sunagawa, Y. Tachikawa, D. Masui, T. Shimada, S. Takagi, D.A. Tryk, Y. Nabetani, H. Tachibana, H. Inoue, J. Catal. 310 (2014) 57.